IEEE Access
Multidisciplinary | Rapid Review | Open Access Journal

Received October 10, 2019, accepted October 20, 2019, date of publication October 31, 2019, date of current version November 19, 2019.

Digital Object Identifier 10.1109/ACCESS.2019.2950725

A New Path Evaluation Method for Path Planning With Localizability

YANG GAO[1,2], JIANG LIU[1], MENG QI HU[2], HAO XU[1], KUN PENG LI[1], AND HUI HU[1]

[1]School of Automobile, Chang'an University, Xi'an 710064, China
[2]Department of Mechanical and Industrial Engineering, The University of Illinois at Chicago, Chicago, IL 60607, USA

Corresponding author: Jiang Liu (tust1314@126.com)

This work was supported in part by the National Natural Science Fund under Grant 61503043, in part by the Natural Science Foundation of Shaanxi Province under Grant 2019JLP-07 and Grant 2017JM7016, and in part by the Foundation of Central University under Grant 310822172204 and Grant 3100102229103.

ABSTRACT As a fundamental capability of mobile robots, path planning highly relies on the accurate localization of the robot. However, limited consideration for the localizability (which describes the capability of acquiring accurate localization) has been made in path planning. This brings a high risk of choosing a path that is optimal but results in the robot easily getting lost. There exist two key challenges to address this problem: 1) How to evaluate the localizability of a path and its impact on path planning. 2) How to balance the localizability of a path and the standard path planning criteria (e.g., shortest travel distance, obstacle-free path, etc.. To overcome the two challenges a new path evaluation method is required. So we first analyzed the uncertainty that comes from dead-reckoning and map matching. Then the localizability was estimated by the fusion of the uncertainty coming from both of them. Based on that, the impact of the localizability on the path planning task has been evaluated by an evaluation function. By combining the localizability evaluation function with traditional criteria (e.g., shortest length, obstacle-free path, etc.), a new path evaluation function for path planning is established. Both simulation and experimental studies show that the new path evaluation function can offer a balance between the localizability and the traditional criteria for path planning.

INDEX TERMS Path planning, localizability, map matching, mobile robot.

I. INTRODUCTION

As one of the fundamental functions of mobile robots, path planning provides the capability to find an optimal path in complex environments from a given start point to the destination, so that many kinds of missions can be carried out. For decades, path planning has attracted plenty of attention with most existing research focused on finding the optimal path according to various criteria including the shortest length, least time [1] or least energy consumption [2], path smoothness, obstacle-free path, ease of implementation, better adaptability to dynamic environments [3], [4], smallest amount of environmental information requests, etc. However, to the best of our knowledge, the localizability of a path has been less of a consideration. This poses a critical challenge for path planning that the planning result may not applicable.

The associate editor coordinating the review of this manuscript and approving it for publication was Nagarajan Raghavan.

A. BACKGROUND OF PATH PLANNING

The existing path planning research can be divided into three categories: global path planning, local path planning, and hybrid path planning.

Global path planning attempts to find an optimal path with a global view of the environment. They generally employ the path evaluation criteria as described above. Traditional graphic search approaches (e.g., A*, D*, D* lite) are a group of commonly used global path planning algorithms. One of the most recent improvements to the A* algorithm was proposed by Guruji *et al.* [5], where the heuristic function's value was only calculated before the collision phase for better efficiency. Sampling-based algorithms are another widely accepted group. Zhang H et al. have recently proposed an enhanced RRT (Rapidly-Exploring Random Tree) algorithm, which has incorporated a regression mechanism for better efficiency. Gao et al. developed an online global path planning algorithm for dynamic environments, which models the global optimal path as a dynamically changing state and employs Particle Filters to track it [3]. Intelligent algorithms

based global path planning methods, such as Neural Network based group, Ant Colony algorithm based group, Particle Swarm Optimization algorithm and Genetic Algorithm based groups also attracted great attention due to their superior performance. Some of their most recent developments can be found in [6]–[9] where efforts have been made in improving the pheromone diffusion approach, the initializing process, and better neural network for better performance separately. Other than those, Seyedhadi Hosseininejad et al. employed a cuckoo optimization algorithm to get a short, safe and smooth path in a dynamic environment [10]. Andrey V. Savkin proposed an efficient method to construct a low-risk aircraft path which can balance the requirements of the low threat level and the short path by employing a geometric procedure to find the shortest path among threat fields [11]. However, most of the exiting researches ignored the influence of localizability, which is this paper mainly focused on.

Local path planning generally relies on local environmental information and provides mapping from that to the behavioral command. The potential field approach, VFF (Virtual Force Field) and VFH (Vector Field Histogram) approaches are three widely known local path planning algorithms that help the robot move along the gradient of a potential field or gaps between obstacles. Their most recent developments can be found in [12], [13], where time variant environments and trap problems have been considered. Ulises Orozco-Rosas proposed a membrane evolutionary artificial field path planning method where a Genetic Algorithm and APF is blended through a membrane structure, to provide feasible and efficient paths in both static and dynamic environments [14]. Farhad Bayat assigned a potential function for each obstacle and integrating all scattered obstacles in a scaler potential surface to obtain an optimal and robust path, which can trade-off between traversing the shortest path and avoiding collisions [15]. Artificial intelligence methods like fuzzy logical control and neural network are also employed in local path planning. Some of their most recent developments can be found in [16] and [13]. Ashanie Gunathillake et al. proposed a navigation algorithm for source seeking in a sensor network environment where the robot is localized in a topology coordinates system based on a packet reception probability function and a packet reception binary matrix [17]. Local path planning approaches are generally efficient enough to be executed online and are capable of dealing with time variant situations. This group of methods generally employ motion evaluation criteria instead of the path evaluation criteria. The most common criteria include: the angle difference or distance between the robot and the target, the angle difference or distance between the robot and the obstacles and these criteria also do not take into consideration the localizability issue either.

Hybrid path planning combines both the global and local path planning approaches, thereby avoiding their drawbacks while retaining their benefits. Li et al. proposed a hybrid approach where a genetic algorithm is used for global path planning and a local rolling optimizer is employed to optimize the global planning results [18]. Madjid and Moussa proposed another representative hybrid approach which employs a random profile approach (APF) for global path planning and a fuzzy-logic approach for local path planning [19].

Two more recent surveys of path planning research can also be found in the papers proposed by Mac *et al.* [20] and Tzafestas [21]. The first survey mainly focuses on heuristic approaches and the second offers broader coverage to almost all related research topics.

B. BACKGROUND OF LOCALIZABILITY IN PATH PLANNING

Localizability was first studied in the field of coastal navigation by Roy *et al.* [22]. Recently, localizability was studied extensively in the field of localization in wireless network [23]–[25]. But, in this paper we mainly focus on the generally used map based localization method where the robot matches the environmental information with the given map combined with dead-reckoning results to localize itself [26]. The early research of this was proposed by Censi, which first offered a theoretical limit to the precision of map matching based localization methods based on Cramér–Rao Bound, while binary map and differentiable obstacles were assumed [27]. From that, a series of localizability researches were then developed. Qian et al. proposed a localizability estimation method by introducing a factor of influence of dynamic obstacles [26], while the localizability matrices in use were derived from the work of Wang *et al.* [28]. A more recent effort on localizability was proposed by Ruiz-Mayor et al. where a probabilistic model of the indistinguishability for perception with different kinds of range sensors was proposed to estimate the perceptual ambiguity [29]. Weikun Zhen et al. also proposed a new method to evaluate the localizability of a given 3D map [30].

Most of the existing path following algorithms highly rely on localization results of the robot. With the consideration of localizability or the uncertainty in localization, much of research in path planning or motion planning has been made [31]. Wang Y *et al.* proposed an effort in developing better motion selection mechanisms to improve localization accuracy [28]. Chen *et al.* presented an algorithm of path planning for a mobile manipulator based on localizability. They used the theory from Censi [27] to evaluate the localizability. Then an evaluation of the localizability of a path was done by accumulating the fisher matrix, multiplied with the derivatives along the path [32]. Robert S *et al.* proposed a path planning algorithm considering the uncertainty of the localization of the path by accumulating a special designed uncertainty evaluation along the path [33]. Behnam Irani *et al.* proposed a LM (localizability measure) method to exclude poorly located areas based on a manual threshold, but only map matching based localizability was considered [34]. Li GQ *et al.* proposed a method to integrate the path planning algorithm with Simultaneous Localization and Mapping (SLAM) algorithm where path length and map

utility are leveraged to reduce the uncertainty in state estimation [35].

To the best of our knowledge, current research in localizability is mostly done for one specific pose only, rather than for that of a path, and is mostly concerned with the uncertainty that comes from map matching or environment observation only. This ignores the influence of dead-reckoning that is generally used in the localization methods as well. Moreover, in most existing research, the uncertainty or localizability is incorporated directly, while their impact on the path planning task has not been incorporated. So, this paper focuses on two key challenges to bridge the gap between localizability and path planning: 1) How to characterize the localizability of a path and its impact on path planning and 2) How to balance the path localizability and the standard path planning criteria (e.g., shortest travel distance, obstacle free).

In this research, we focused on a differential driven robot equipped with LIDAR and encoder. Firstly, we will analyze the localizability that comes from dead-reckoning and map matching. Secondly, commonly used localization method will be analyzed to fuse the results from dead-reckoning and map matching. Thirdly, an impact evaluation function of uncertainty of the localization of any one pose on the path will be introduced. This will be analyzed in detail in another paper. Finally, we will propose a new evaluation function for a path to bridge the existing localizability research and the path planning.

This paper is organized as follows: Section 2 discusses the localizability and its impact. Section 3 offers a new path evaluation function considering localizability. Section 4 offers a series of simulations to prove the performance. Section 5 offers an experiment running in a closed environment. Finally, conclusions are drawn in Section 6. Table 1 shows the symbols used in this paper.

TABLE 1. Symbols in use.

Symbol	The mean of the symbol
S	2D Pose of the robot
S_{d_k}	Estimation of the S based on dead-reckoning
S_{m_k}	Estimation of the S based on map matching
S_{f_k}	Estimation of the S after the fusion of both S_{d_k} and S_{m_k}
s	Subscript, means the corresponding value of the pose estimation of the robot
x, y, θ	X , Y coordinates and orientation of the robot
k	current time step
$A \sim N(\overline{A}, \delta_A)$	A conforms a Gaussian distribution whose mean is $\overline{A}$, covariance is $\delta_{\overline{A}}$
δ	Covariance
δ_{d_sk}	Covariance of the estimation based on dead-reckoning
δ_{m_s}	Covariance of the estimation based on map matching
δ_{f_s}	Covariance of the estimation after the fusion of both δ_{d_sk} and δ_{m_s}
$v,\ \omega$	Linear velocity and angular velocity of the robot
δ_{f_xy}	The covariance of the estimation of X-Y coordinates of the robot
$\delta_{\mathrm{f}\_\theta}$	The variance of the estimation of θ of the robot
Δt	Time span between two time steps
$\|\delta\|$	The half length of the longer axis of the distribution ellipse of the given covariance
$\|\delta_{\mathrm{f}\_D}\|$	The half length of the longer axis of the distribution of ellipse of δ_{f_xy}
$\|\delta_{\mathrm{m}\_D}\|$	The half length of the longer axis of the distribution of ellipse of δ_{m_xy}
δ_{p}	Variance of the observation noise of the laser range finder
δ_{e}	Covariance of the Gaussian noise comes with the dead-reckoning.
R_d	Turning radius of the motion of the robot
R	Turning radius of the motion of the path
r_s	Turning radius of the motion of the robot
r_{a}	Turning radius of the motion of the path
r_R	The safe radius of the robot.
L	Turning radius of the motion of the path
$\Delta\theta_{\mathrm{T}}$	The angle difference between the orientation and the target of the motion.
$E_\theta(\bullet)$	Evaluation function for $\delta_{\mathrm{f}\_\theta}$ and $\delta_{\mathrm{m}\_\theta}$
$E_{\max}$	Maximum evaluation along the path R
$E(\|\delta_{\mathrm{f}\_D}\|)$	Evaluation function for $\|\delta_{\mathrm{f}\_D}\|$
$E(\|\delta_{\mathrm{m}\_D}\|)$	Evaluation function for $\|\delta_{\mathrm{m}\_D}\|$
r_i	The ith Ferguson spline in the path
k_p	The index of the of the sample positions along the path
K	The number of the sample positions along the path
i	The index of the Ferguson spline in the path

II. THE LOCALIZABILITY AND ITS IMPACT

A. THE UNCERTAINTY IN LOCALIZATION

In practice, a robot generally needs to localize itself while following a path R. The final localization result and the uncertainty of the localization come from the fusion of two localization results: the dead-reckoning and the map matching. A Kalman filter is generally employed in the information fusion task as well as in the localization task. So, the localization task may also be treated as a fusion task. Fusing the pose estimation comes from both the dead-reckoning and the map matching.

The research in [31] has offered a theoretical analysis for the uncertainty which comes from the dead-reckoning. But here we offer a simplified version instead for better efficiency. As it is shown in table 1, let $S_k(x_k, y_k, \theta_{k-1})$ be the current pose of the robot and the current state of the Kalman filter as well. Its estimation after the fusion of both dead-reckoning and map matching is $S_{\mathrm{f}\_k} \sim N(S_k, \delta_{\mathrm{f}\_sk})$. Then formula (1) shows the dead-reckoning formula used in the Kalman filter where $f()$ is the motion model of the robot, $e_k \sim N(0, \delta_e)$ is the 0 mean Gaussian noise, which comes with the dead-reckoning, u_k is the motion of the robot. For differential robot u_k is the motion information, then $f()$ can be obtained from the motion model of differential robot as shown in formula (2)-(3) [36]. Fig.1 also shows the motion model. Assume the estimation of S_k based on dead-reckoning is $S_{\mathrm{d}\_k} \sim N(S_k, \delta_{\mathrm{d}\_sk})$. Then according to formula (1), δ_{d_sk} can be obtained as shown in formula (4). Moreover,

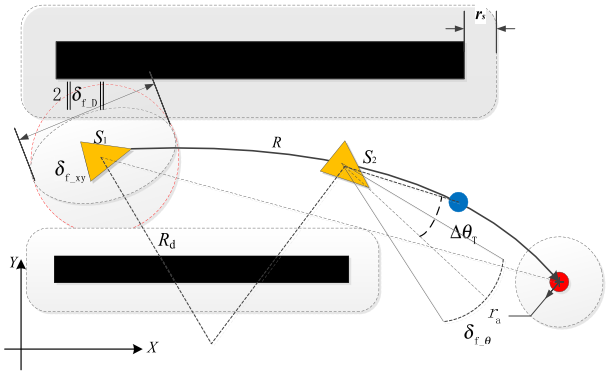

FIGURE 1. The uncertainty in localization.

based on formula (2)- (3), $\frac{\partial f}{\partial s}$ can be gotten by formula (5).

$$S_k = f(S_{k-1}, u_k) + e_k \tag{1}$$

$$\begin{aligned} x_k &= x_{k-1} - R_d \sin\theta_{k-1} + R_d \sin(\theta_{k-1} + \omega_{k-1}\Delta t) \\ y_k &= y_{k-1} + R_d \cos\theta_{k-1} - R_d \cos(\theta_{k-1} + \omega_{k-1}\Delta t) \\ \theta_k &= \theta_{k-1} + \omega_{k-1}\Delta t \end{aligned} \tag{2}$$

$$R_d = \frac{v_{k-1}}{\omega_{k-1}} \tag{3}$$

$$\delta_{d\_sk} = \frac{\partial f}{\partial s}\delta_{f\_sk-1}\frac{\partial f'}{\partial s} + \delta_e \tag{4}$$

$$\frac{\partial f}{\partial s} = \begin{pmatrix} \frac{\partial f}{\partial x} \\ \frac{\partial f}{\partial y} \\ \frac{\partial f}{\partial \theta} \end{pmatrix} = \begin{pmatrix} 1 - \frac{\partial R_d}{\partial x_{k-1}}(\sin\theta_{k-1} - \sin(\theta_k)) \\ 1 + \frac{\partial R_d}{\partial y_{k-1}}(\cos\theta_{k-1} - \cos(\theta_k)) \\ 1 + \frac{\partial \Delta\theta}{\partial \theta_{k-1}} \end{pmatrix} \tag{5}$$

Here, R_d is the turning radius of the robot in path following at pose$(x_{k-1}, y_{k-1}, \theta_{k-1})$. $\frac{\partial R_d}{\partial x_{k-1}}$, $\frac{\partial R_d}{\partial y_{k-1}}$ can be safely treated as a derivation of the curvature of the path along X and Y axis separately, by ignoring the inaccurate motion in the path following. Then the impact of $\frac{\partial R_d}{\partial x_{k-1}}$, $\frac{\partial R_d}{\partial x_{k-1}}$, $\frac{\partial \Delta\theta}{\partial \theta_{k-1}}$ is roughly ignored here. The deviation from the real value of the uncertainty caused by that ignorance is big only while both the R_d and θ changed sharply. So that formula (4) can be simplified to formula (6).

$$\delta_{d\_sk} = \delta_{f\_sk-1} + \delta_e \tag{6}$$

The theory of localizability proposed by Censi [27], Wang *et al.* [28] has in fact proposed a good method to estimate the uncertainty, which comes from map matching based localization. WANG Wei et al extended it to the probabilistic grid map and proposed Static Localizability as the formula (7), which offers a mathematically way to describe the influence caused by environmental information and map noises [37]. So, we simply employ the theory to estimate the uncertainty that comes from map matching. In formula (7), r_{iE} is the expected distance between the LIDAR and obstacle measured by the i_{th} ray. Assume the estimation S based on the map matching is $S_m \sim N(S, \delta_{m\_s})$. Then according to [27], [28] we can get the lower bound of its covariance δ_{m_s} as shown in formula (8), which represents the localizability at S with map matching using LIDAR.

$$\begin{aligned} I(S) &= \frac{1}{\delta_p}\sum_{i=1}^{n}\left[\frac{\partial r_{iE}}{\partial S}^T \frac{\partial r_{iE}}{\partial S}\right] \\ &= \frac{1}{\delta_p}\sum_{i=1}^{n}\begin{bmatrix} \frac{\Delta r_{iE}^2}{\Delta x^2} & \frac{\Delta r_{iE}^2}{\Delta x \Delta y} & \frac{\Delta r_{iE}^2}{\Delta x \Delta \theta} \\ \frac{\Delta r_{iE}^2}{\Delta x \Delta y} & \frac{\Delta r_{iE}^2}{\Delta y^2} & \frac{\Delta r_{iE}^2}{\Delta y \Delta \theta} \\ \frac{\Delta r_{iE}^2}{\Delta x \Delta \theta} & \frac{\Delta r_{iE}^2}{\Delta y \Delta \theta} & \frac{\Delta r_{iE}^2}{\Delta \theta^2} \end{bmatrix} \end{aligned} \tag{7}$$

$$\delta_{m\_s} \geq \frac{1}{I(S)} \tag{8}$$

B. THE LOCALIZABILITY OF THE LOCALIZATION WITH BOTH DEAD-RECKONING AND MAP MATCHING

As $S_f \sim N(S, \delta_{f\_s})$, δ_{f_s} defines an ellipsoid shape probability distribution space of the pose of the robot. Let δ_{f_xy} denotes the covariance of the estimation of the X-Y coordinates of the robot, δ_{f_θ} denotes the variance of the estimation of θ, then δ_{f_s} can be expressed as $(\delta_{f\_xy}, \delta_{f\_\theta})$. Similarly, δ_{f_xy} defines an ellipse shape probability distribution area. In fig.1, the triangles denote the poses of the robot, while the dashed ellipse around each of them shows the ellipse of δ_{f_xy} and the solid line denotes the given path. To tolerate the inaccurate motion and localization, all obstacles are generally inflated by a safe radius r_s. Similarly, the destination is also generally inflated by r_a to tolerate the inaccurate localization. Fig.1 shows the obstacles in black, the destination in red, and the inflated regions of them in dashed lines around them.

According to the data fusion theory, the covariance δ_{f_s} could be simplified to formula (9) if a Kalman filter is employed. Moreover, δ_{f_s} would satisfy formula (10), which means that the fusion result cannot be worse than the dead-reckoning estimation and the map matching one either.

$$\delta_{f\_s} = (\delta_{d\_s}^{-1} + \delta_{m\_s}^{-1})^{-1} \tag{9}$$

$$\delta_{f\_s} \leq \min(\delta_{d\_s}, \delta_{m\_s}) \tag{10}$$

Let $\|\delta_{f\_D}\|$ denotes the half length of the longer axis of the ellipse of δ_{f_xy}. According to the knowledge of bivariate normal distribution, one can easily see that if $1-\alpha$ is the probability that the robot is located inside the ellipse of δ_{f_xy}, then $\|\delta_{f\_D}\|$ can be gotten by formula (11). Here $\chi_2^2(\alpha)$ is the upper (100α)th percentile of a χ^2 distribution with 2 degrees of freedom and λ_{max} is the biggest eigenvalue of δ_{f_xy}. In this paper we simply choose $\chi_2^2(\alpha) = 1$. So, in terms of the risk of inaccurate localization, δ_{f_xy} can be represented by its ellipse while the probability that the robot is located outside the ellipse is α. Note that the impact of the localizability to path planning mainly comes from the inaccurate localization result. As we cannot predict the relationship between the obstacle and the ellipse, it would be difficult to evaluate the impact of the ellipse to path planning. On the other hand, to cover the ellipse of δ_{f_xy}, we can define a circle region whose radius is $\|\delta_{f\_D}\|$ with the center at (x_k, y_k) as the red

dashed circle showed in fig.1. This circle defines a region that the robot is most likely located inside and would be easier to be used in evaluating its impact to path planning. Like the ellipse of $\delta_{\mathrm{f\_xy}}$, the probability that the robot is locating inside this circle region, is no less than $1-\alpha$. So, in terms of the risk of inaccurate localization, the risk defined by $\delta_{\mathrm{f\_xy}}$ can be safely covered by the circle region, which can be measured by $\|\delta_{\mathrm{f\_}D}\|$. Then we can say that the impact of $\delta_{\mathrm{f\_}s}$ can be measured by $(\|\delta_{\mathrm{f\_}D}\|, \delta_{\mathrm{f\_}\theta})$.

$$\|\delta_{\mathrm{f\_}D}\| = \sqrt{\chi_2^2(\alpha)\lambda_{\max}} \tag{11}$$

C. THE IMPACT OF THE LOCALIZABILITY OF A POSE ON PATH PLANNING

Here we offer a brief analysis on the impacts of $\|\delta_{\mathrm{f\_}D}\|$ and $\delta_{\mathrm{f\_}\theta}$, while the detailed analysis was proposed in another paper [38].

1) THE IMPACT OF $\|\delta_{\mathrm{f\_}D}\|$

In path planning, the optimal path is generally close to obstacles for shorter length. So, a pose with bigger $\|\delta_{\mathrm{f\_}D}\|$ will bring a bigger risk of collision with the obstacles due to inaccurate localization result. This means the bigger the $\|\delta_{\mathrm{f\_}D}\|$ of the pose is, the worse the path that contains the pose will be. Furthermore, to reduce the risk of collision, $\|\delta_{\mathrm{f\_}D}\|$ should satisfy formula (12). Formula (12) means the uncertainty of localization should be within the tolerance provided by both r_R and r_s. To reduce the risk that the robot cannot reach the destination due to the inaccurate localization result, formula (13) should also be satisfied, which means the uncertainty of the localization should not exceed the given tolerance range r_{a}.

$$r_s > \|\delta_{\mathrm{f\_}D}\| + r_R \tag{12}$$

$$\|\delta_{\mathrm{f\_}D}\| < r_{\mathrm{a}} \tag{13}$$

2) THE IMPACT OF $\delta_{\mathrm{f\_}\theta}$

The motion control algorithms of the robot always try to reduce the difference between the orientation of the robot and the destination (or the current target). Let $\Delta\theta_{\mathrm{T}}$ denote the angle difference between the orientation and the destination (or the current target), then the motion control of the robot towards the orientation can be simplified as formula (14). Fig.1 shows the $\Delta\theta_{\mathrm{T}}$ and the current target as the blue dot. The parameter γ may differ in different control policies. As we ignore the limited turning capability of the robot here, then $\gamma = 1$.

$$\theta_k = \theta_{k-1} - \gamma\Delta\theta_T \tag{14}$$

As the estimation of θ_{k-1} is $\theta_{\mathrm{f}\_k-1} \sim N(\theta_{k-1}, \delta_{\mathrm{f\_}\theta k-1})$, according to the knowledge of variance, with the probability at about 0.683 we have $\theta_{k-1} - \delta_{\mathrm{f\_}\theta k-1} \le \theta_{\mathrm{f}\_k-1} \le \theta_{k-1} + \delta_{\mathrm{f\_}\theta k-1}$. Assuming the estimation error of θ_{f_k-1} always reaches $\delta_{\mathrm{f\_}\theta k-1}$, then we can set $\theta_{\mathrm{f}\_k-1} = \theta_{k-1} + \delta_{\mathrm{f\_}\theta k-1}$. So, we can get the estimation $S_{\mathrm{f}\_k}(x_{\mathrm{f}\_k}, y_{\mathrm{f}\_k}, \theta_{\mathrm{f}\_k})$ using the motion model of the robot as formula (15). Here v is the moving speed of the robot in following the path and Δt is the time step.

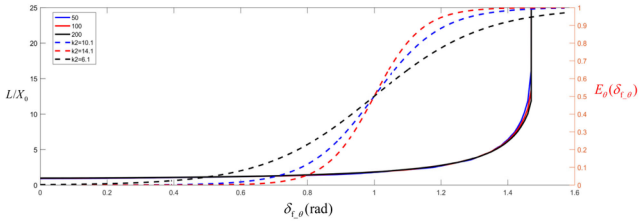

FIGURE 2. $\frac{L}{X_0}$ and $\delta_{\mathbf{f\_}\theta}$ with different X_0, $E_\theta(\delta_{\mathbf{f\_}\theta})$ and $\delta_{\mathbf{f\_}\theta}$ with different k_2.

$$\begin{aligned} x_{\mathrm{f}\_k} &= x_{\mathrm{f}\_k-1} + v\Delta t\cos(\theta_{\mathrm{f}\_k}) \\ y_{\mathrm{f}\_k} &= y_{\mathrm{f}\_k-1} + v\Delta t\sin(\theta_{\mathrm{f}\_k}) \\ \theta_{\mathrm{f}\_k} &= \theta_{\mathrm{f}\_k-1} + \delta_{\mathrm{f\_}\theta k-1} - \Delta\theta_T \end{aligned} \tag{15}$$

Assuming the robot starts at $S_0(X_0, 0, 0)$ and $r_{\mathrm{a}} = 5$, then according to formula (15), we can get the path from S_0 to the destination. The three solid lines in blue, red and black shown in fig.2 describe the relationships between $\frac{L}{X_0}$ and $\delta_{\mathrm{f\_}\theta}$ with X_0 =(50cm,100cm, 200cm) separately. It can be found that if $\delta_\theta \ge \frac{\pi}{2}$, the path will never reach the destination. By adjusting the X_0, it can also be found that there is a similar relationship between $\frac{L}{X_0}$ and $\delta_{\mathrm{f\_}\theta}$.

D. EVALUATION FUNCTION FOR THE IMPACT OF $\|\delta_{f\_D}\|$

An evaluation function is generally required in path planning in order to map the impact to a limited value domain. Meanwhile, a differentiable evaluation function may be preferred by some path planning approaches. So, according to the prior impact analysis, a sigmoid function is employed to evaluate the impact of $\|\delta_{\mathrm{f\_}D}\|$ of pose S.

Our evaluation function $E(\|\delta_{\mathrm{f\_}D}\|)$ represents the evaluation of $\|\delta_{\mathrm{f\_}D}\|$ as formula (16) while the smaller the value of $E(\|\delta_{\mathrm{f\_}D}\|)$ is the better. Here r_u is the lowest limitation defined by formula (17), which comes from the relationship defined in formulas (12) and (13). Parameter k_1 defines the raising ratio of the evaluation value. Fig. 3 shows 6 dashed curves representing the relationship between $\|\delta_{\mathrm{f\_}D}\|$ and $E(\|\delta_{\mathrm{f\_}D}\|)$ with $k_1 = 0.2, 0.6, 1, 2, 3, 4$ separately. Moreover, k_1 should be set to make $E(r_u) \approx 1$. In this paper, we set $k_1 = 1$, $r_s = 50$cm, $r_R = 30$cm, $r_{\mathrm{a}} = 50$cm.

$$E(\|\delta_{\mathrm{f\_}D}\|) = sig(\|\delta_{\mathrm{f\_}D}\|) = \frac{1}{1+e^{-k_1(\|\delta_{\mathrm{f\_}D}\| - \frac{r_u}{2})}} \tag{16}$$

$$r_{\mathrm{u}} = \min(r_s - r_R, r_{\mathrm{a}}) \tag{17}$$

E. EVALUATION FUNCTION FOR THE IMPACT OF δ_{f_θ}

As shown in fig.2, $\delta_{\mathrm{f\_}\theta}$ shows a negative impact on the path. So the evaluation function $E_\theta(\delta_{\mathrm{f\_}\theta})$ as shown in formula (18) is created, while the smaller the value of $E_\theta(\delta_{\mathrm{f\_}\theta})$ is, the better. Here, θ_{u2}, the manually adjusted parameter, comes from the truth that the robot can never reach the destination with

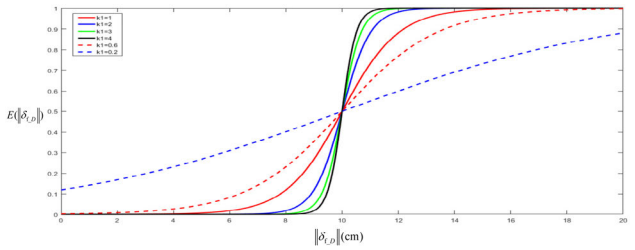

FIGURE 3. Different evaluation $E(\|\delta_{f\_D}\|)$ with different k_1 and different $\|\delta_{f\_D}\|$.

$\delta_\theta \geq \frac{\pi}{2}$ and $E_\theta(\frac{\theta_{u2}}{2}) = 0.5$. Parameter k_2 defines the raising ratio of the evaluation value and should be manually adjusted. The dash curves in fig.2 show the relationships between $E_\theta(\delta_{f\_\theta})$ and δ_{f_θ}, using the right vertical axis, with $\theta_{u2} = 2$, k_2 is set to 6.1, 10.1 and 14.1 separately. In this paper we set $k_2 = 14.1$, $\theta_{u2} = 2$ so that $E_\theta(1) = 0.5$ and $E_\theta(1.4) \approx 1$.

$$E_\theta(\delta_{f\_\theta}) = sig(\delta_{f\_\theta}) = \frac{1}{1 + e^{-k_2(\delta_{f\_\theta} - \frac{\theta_{u2}}{2})}} \tag{18}$$

III. PATH EVALUATION CONSIDERING LOCALIZABILITY

A. PATH DESCRIPTION

Ferguson splines are employed to describe the path for the robot due to their smoothness and the convenience in path following as it has been done in our prior research [3]. So path R is described as n smoothly connected *Ferguson* splines $r_i(i = 1 \ldots n)$ that are defined by several points and tangent vectors. As a result, R is defined by a set of points and tangent vectors like $R\{P_0, P_0' \ldots P_n, P_n'\}$. Here P_{i-1} and P_i are the start point and the end point of the *Ferguson* spline r_i which is a part of R. P_{i-1}' and P_i' are the tangent vectors at P_{i-1} and P_i respectively.

B. NEW EVALUATION FUNCTION CONSIDERS LOCALIZABILITY FOR PATH PLANNING

For a path R, an evaluation function $E(R, MC)$ is created in [3], which represents the traditional requirements for paths that are shorter and further away from the obstacle. To reduce the impact of the localizability, the $E(R, MC)$ is enlarged to a new path evaluation function $E_p(R, MC)$ as shown in formula (19). It can be found that only $E_{L\max}(R)$ has been added into the $E(R, MC)$ to introduce the localizability requirement into path planning. Here MC is the map of the environment, L is the length of R defined by formula (22), $l_{\min}$ is the minimum path length between the start point P_0 and the destination Ta. $d_{\min}$, defined by formula (23), is the minimum distance from R to obstacles, α_1 is a weight parameter. $X_i(T)$ and $Y_i(T)$ are the coordinates X and Y of spline i respectively. $X_i'(T)$ and $Y_i'(T)$ are the derivations of $X_i(T)$ and $Y_i(T)$ to parameter $T \in [0, 1]$, respectively. obj_x and obj_y in formula (23) are the coordinates X and Y of the closest obstacle point. $E_{L\max}(R)$ is the maximum localizability evaluation value in all the poses along R as shown in formula (20) where $E_s(S)$, shown in formula (21), is the localizability evaluation of a given pose S. $\alpha_1, \alpha_2, \alpha_3$ are the three weights for the influences of $d_{\min}$, $\|\delta_{f\_D}\|$ and δ_{f_θ}, respectively.

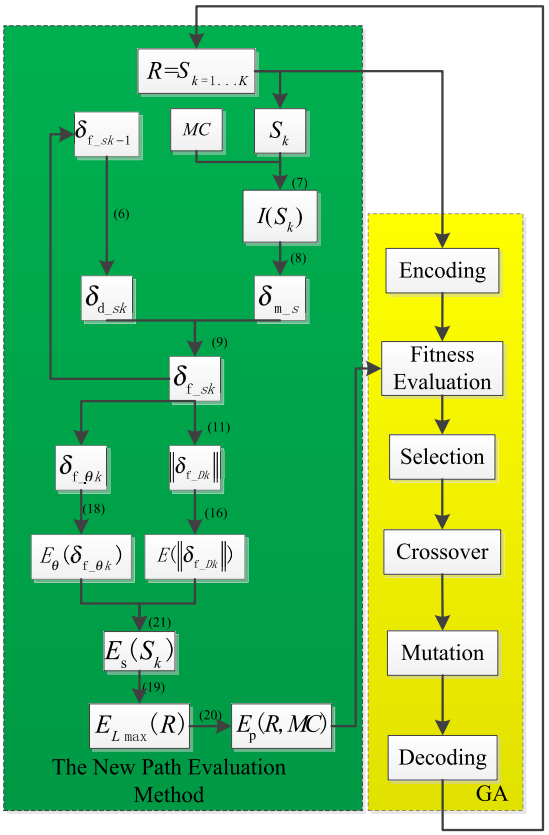

FIGURE 4. The flowchart of path planning with our evaluation function.

$$E_p(R, MC) = \begin{cases} \frac{L}{l_{\min}} + \frac{\alpha_1}{d_{\min}} + E_{L\max}(R) & R \text{ is feasible} \\ E_{\max} & \text{otherwise} \end{cases} \tag{19}$$

$$E_{L\max}(R) = \max(E_S(S)) | \forall S \in R \tag{20}$$

$$E_S(S) = \alpha_2 E(\|\delta_{f\_D}\|) + \alpha_3 E_\theta(\delta_{f\_\theta}) \tag{21}$$

$$L = \sum_{i=1}^{n} \int_0^1 \sqrt{X_i'(T)^2 + Y_i'(T)^2} dT \tag{22}$$

$$d_{\min} = \min_{\substack{T\in[0,1] \\ i=1\ldots n}} (\sqrt{(X_i(T) - obj_x)^2 + (Y_i(T) - obj_y)^2}) \tag{23}$$

The left block of fig. 4 shows the flow chart of the mathematic calculation of the new path evaluation function and the formulas involved. As it shows, a path R can be discretized into K poses $S_{k=1\ldots K}$ along the path. For each pose S_k, the Fisher's information matrix $I(S_k)$ can be obtained according to formula (7) and then the localizability with map matching δ_{m_s} can be obtained by formula (8) accordingly. On the other hand, the localizability with dead-reckoning δ_{d_sk} can be obtained according to formula (6) given S_{k-1} is the prior

pose along R. Thus, the localizability after fussing both dead-reckoning and map matching δ_{f_sk} can be obtained according to (9). From δ_{f_sk}, $\delta_{\mathrm{f}\_\theta k}$ and $\left\|\delta_{\mathrm{f}\_Dk}\right\|$ can be obtained to calculate their evaluations $E_\theta(\delta_{\mathrm{f}\_\theta k})$ and $E(\left\|\delta_{\mathrm{f}\_Dk}\right\|)$ separately according to formulas (11), (18) and (16) respectively. So that, as the evaluation of localizability for S_k, $E_s(S_k)$ can be obtained according to formula (21) while $E_{L\max}(R)$ can be obtained according to formula(20). Finally the new evaluation of R, which is $E_{\mathrm{p}}(R, MC)$, can be obtained according to formula (19).

The computational burden of our evaluation function mainly comes from two source. The first is the computation of the δ_{m_s} whose computational burden is $O(N_{\mathrm{f}}n)$ where N_{f} is the number of grids along one laser ray and n is the number of laser rays in each scan. Thus, this computation burden for a path R is $O(N_{\mathrm{f}}nK)$. The second is the computation of $\left\|\delta_{\mathrm{f}\_Dk}\right\|$, which requires a Cholesky factorization for each pose S_k. Thus, this computational burden for R is $O(K)$. Fortunately, the computation of the δ_{m_s} can be computed in advance in a static environment. As a result, the computational burden of our evaluation function for R is $O(K)$.

IV. SIMULATION RESEARCH

To prove the effect of the proposed approach, two comparisons of simulations were run using MATLAB in a typical indoor environment as shown in fig.6**,** where the black dots show the edges of objects. As a popular intelligent global path planning approach with excellent optimization ability, traditional *Genetic Algorithm*(*GA*) was employed. The right block of fig. 4 shows the key steps of *GA*. It can be found that the new path evaluation function is employed as a fitness evaluation function in the Fitness Evaluation step of *GA*. Then in each comparison, two different evaluation functions were employed as the fitness function for *GA* separately. In each comparison the first path planning algorithm has employed the new evaluation function $E_{\mathrm{p}}(R, MC)$ as shown in formula (19), while the second path planning algorithm has employed the traditional evaluation function $E(R, MC)$ as shown in [3]. For better comparison of the different evaluations, the Genetic Algorithm and Direct Search Toolbox of MATLAB was employed in both series of simulations with the same parameter settings. These parameters have included the same path description, which was composed of 4 *Ferguson* splines, the same population size, which was 4000, the same maximum iteration time, which was 100. Some other default genetic operators suggested by the toolbox have been accepted in both series, which included: stochastic uniform selection, scattered crossover etc. Detailed descriptions of these operators are found in the documentation of the toolbox. The three weights $\alpha_1, \alpha_2, \alpha_3$ were set to 4, 1, 1 respectively. The diagonal elements of δ_e were set to (0.1, 0.1, 0.05) respectively. In the following simulations and experiments, maps of $E(\left\|\delta_{\mathrm{m}\_D}\right\|)$ and $E_\theta(\delta_{\mathrm{m}\_\theta})$ are shown separately, where the LIDAR used by the robot is assumed to have a 360° field of view. The grids in those maps show the evaluation values in all the sample positions whose size are 0.05m. The darker the grid is, the higher evaluation value it has.

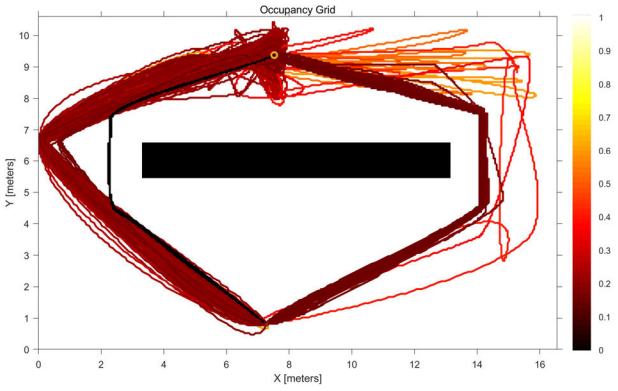

FIGURE 5. Two groups of paths and their fitness values around simple wall.

Figure. 5 shows the performance of our algorithm when facing the local minimal problem. In this situation the start point and the destination are separated by a simple wall, which is represented by the black rectangle. Then with our algorithm, two groups of paths as shown in figure 5, would be found after 100 iterations. In figure 5, each curve represents a path connecting the start point and the destination while the color of the curve represents its normalized evaluation using our new path evaluation function. It can be found that the darker the curve is, the better the path is. So, the group of paths concentrated beside the right side of the wall contains a local minimal which is a sub optimal path. As the capability of dealing with this situation mainly relies on the path planning algorithm adopted to combine with our path evaluation function, *GA* has successfully found the global optimal path.

A. COMPARISON 1 WITH 3M MAXIMUM OBSERVE RANGE

In this simulation, the maximum observation range of the LIDAR is limited to 3m. The so-called traditional optimal path, which is the path planning result using the traditional evaluation function, is shown as the blue solid line in fig.6. It is also shown as a blue solid line in fig.7, where the evaluation map of $E(\left\|\delta_{\mathrm{m}\_D}\right\|)$ is also included. It can be easily found that with the traditional evaluation function, the path planning algorithm seeks for the shortest safe path regardless of the localizability. If we calculate all the four key localizability evaluations $\left\|\delta_{\mathrm{f}\_D}\right\|$, $\delta_{\mathrm{f}\_\theta}$, $E(\left\|\delta_{\mathrm{f}\_D}\right\|)$, $E_\theta(\delta_{\mathrm{f}\_\theta})$ for all the poses along the traditional optimal path, then the localizability evaluations along the path are shown in fig.8. In fig.8(a), the solid red and solid black curves, show the $\left\|\delta_{\mathrm{f}\_D}\right\|$ and the $\delta_{\mathrm{f}\_\theta}$ along the path respectively while the $\left\|\delta_{\mathrm{f}\_D}\right\|$ using the right vertical axis and the $\delta_{\mathrm{f}\_\theta}$ using the left one. In fig.8(b), the dash red and dash black curves, show the $E(\left\|\delta_{\mathrm{f}\_D}\right\|)$ and the $E_\theta(\delta_{\mathrm{f}\_\theta})$ along the path respectively. Note that in all the following figures, the cross in path represents the start

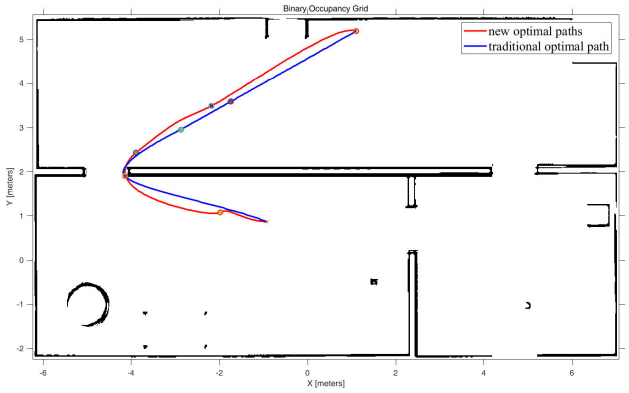

FIGURE 6. The two optimal paths using different evaluation functions.

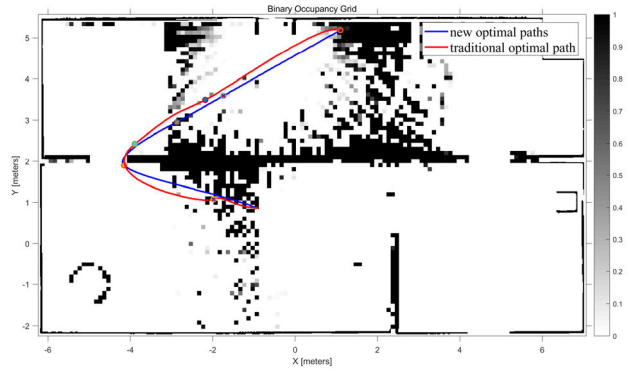

FIGURE 7. The two optimal paths in the map of $E(\|\delta_{m\_D}\|)$.

point of the path, the circles with cross inside represent the connecting points of different Ferguson splines, the circle without the cross inside represents the destination. All the following figures that describe the localizability evaluations will show four curves that represent the same values as they did in fig.8 and the horizontal axis shows the indices k_p of the sample positions along the path.

By employing the new evaluation function in path planning, the localizability is considered and then a so-called new optimal path is gotten, which is also shown in fig.6 using a red curve. Fig.7 shows the two optimal paths coupled with the map of $E(\|\delta_{m\_D}\|)$. It can easily be found that with the help of the new evaluation function, *GA* has avoided the low localizability area, which has been represented by the dark grids, so that the evaluation to the path has been successfully limited. Fig.9 shows all the four localizability evaluations along the new optimal path, where it can be found that the localizability evaluation has been successfully limited to a small value. By comparing fig.8 and fig.9, it can also be found that the localizability is mainly refined by $E(\|\delta_{m\_D}\|)$, which is much higher than $E_\theta(\delta_{m\_\theta})$ and the tail parts of the two optimal paths show great differences, where the traditional one endures a much higher localizability evaluation close to 0.6. Finally, with our new evaluation function, the traditional optimal path gets a new evaluation value 2.8863, while,

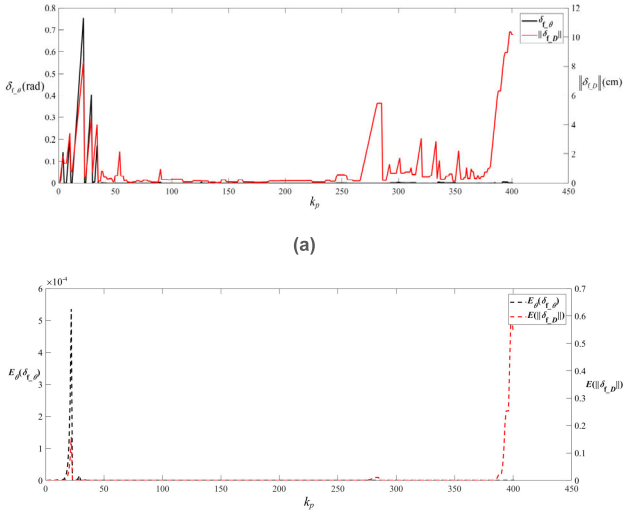

FIGURE 8. (a)δ_{f_θ} and $\|\delta_{f\_D}\|$ along the traditional optimal path. (b) $E_\theta(\delta_{f\_\theta})$ and $E(\|\delta_{f\_D}\|)$ along the traditional optimal path.

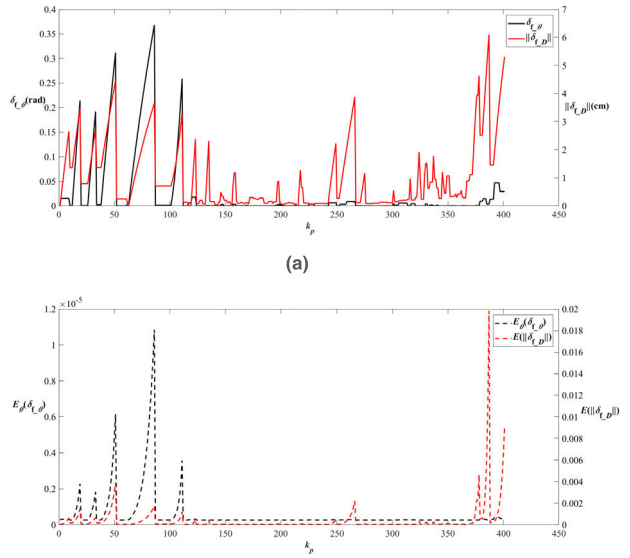

FIGURE 9. (a) δ_{f_θ} and $\|\delta_{f\_D}\|$ along the new optimal path. (b) $E_\theta(\delta_{f\_\theta})$ and $E(\|\delta_{f\_D}\|)$ along the new optimal path.

in contrast, the new optimal path gets a much lower new evaluation value 2.3543.

B. COMPARISON 2 WITH 2M MAXIMUM OBSERVATION RANGE

A smaller maximum observation range brings more challenges to the robot due to its lessened capability to capture sufficient references for the localization task. So, as shown in fig.10, the red curve shows a more complex new optimal path than the blue one, which is the traditional optimal path. Fig.11 shows the two optimal paths with the map of $E(\|\delta_{m\_D}\|)$. The new optimal path seems more complex because it makes more adjustments to avoid moving too

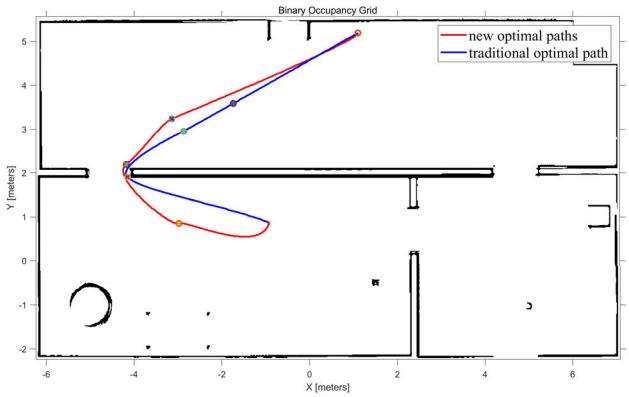

FIGURE 10. The two optimal paths using different evaluation functions.

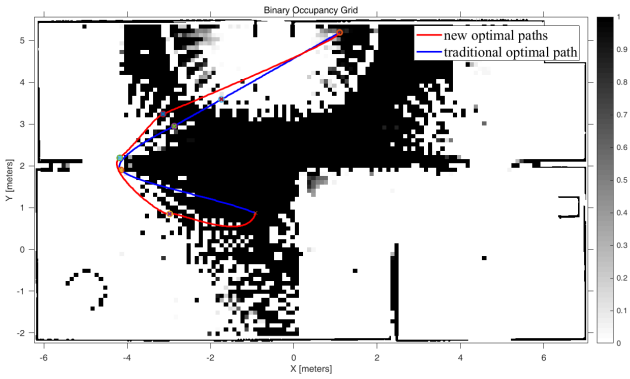

FIGURE 11. The two optimal paths in map of $E(\|\delta_{m\_D}\|)$.

long a distance in the dark area of $E(\|\delta_{m\_D}\|)$ map, which would bring sustained raising of the localizability evaluation. As a result, the localizability evaluations of the new optimal path in fig.12 show that the $E(\|\delta_{f\_D}\|)$, which is the biggest localizability evaluation, has been limited to less than 0.14.

In comparison, the traditional optimal path endures worse localizability for its lack of consideration to the localizability. As the localizability evaluations in fig.13 showed, the $E(\|\delta_{f\_D}\|)$ of the traditional optimal path reaches 1, which means the robot probably cannot keep safe in path following due to the too big uncertainty in localization. Taking the $E(\|\delta_{f\_D}\|)$ for instance, according to fig.11 to fig. 13, it can be found that the traditional path brings sustained raising of $E(\|\delta_{f\_D}\|)$ when it traverses through the black region in fig. 11 for too long a distance.

On the other hand, the new optimal path moves out of the black region when the $E(\|\delta_{f\_D}\|)$ and $E_\theta(\delta_{f\_\theta})$ have risen too much in cost of a longer length. Finally, evaluated by the new evaluation function, the new optimal path gets a new evaluation value of 2.69 while the traditional path gets a new evaluation value of 4.3.

V. EXPERIMENT STUDY

In this section, we first introduced the experimental platform that was used in two indoor experiments, which included one simple environment and one complicated environment. In the

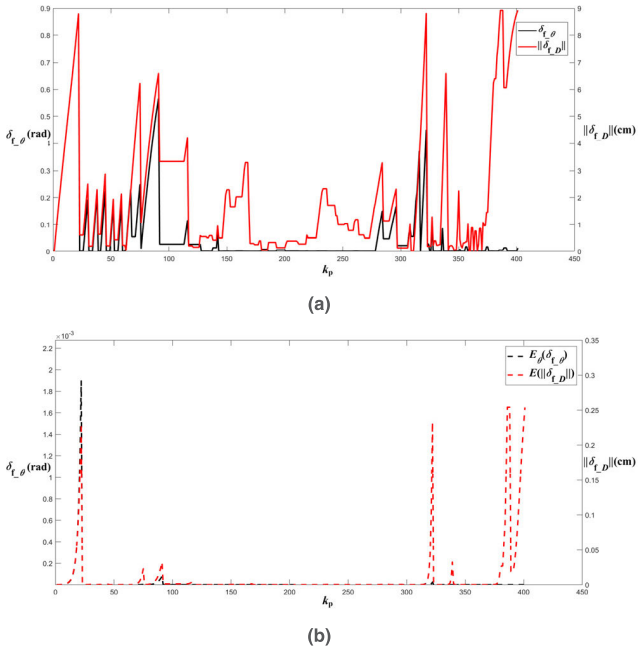

FIGURE 12. (a) δ_{f_θ} and $\|\delta_{f\_D}\|$ along the new optimal path. (b) $E_\theta(\delta_{f\_\theta})$ and $E(\|\delta_{f\_D}\|)$ along the new optimal path.

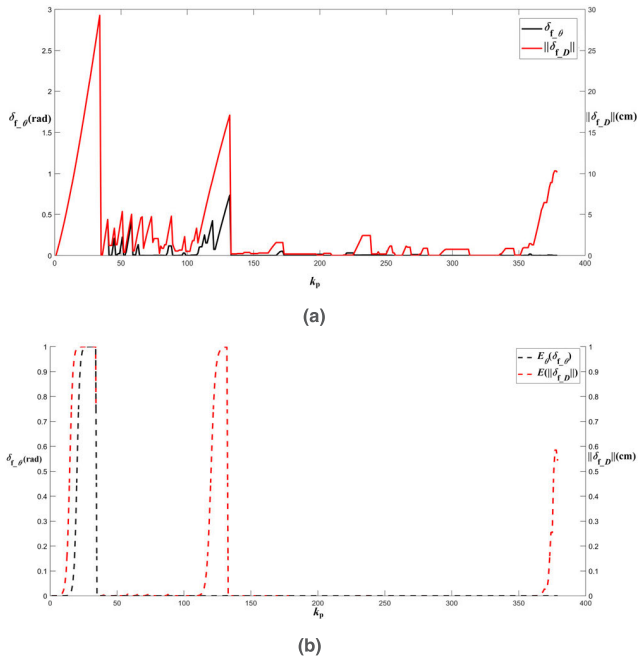

FIGURE 13. (a) δ_{f_θ} and $\|\delta_{f\_D}\|$ along the traditional optimal path. (b) $E_\theta(\delta_{f\_\theta})$ and $E(\|\delta_{f\_D}\|)$ along the traditional optimal path.

two experiments, we added the LM Method proposed in [34] for comparison. Because the LM Method has also employed the theory proposed by Censi to evaluate the localizability while the evaluation is considered in path planning. In all situations, *GA* was employed in path planning.

A. EXPERIMENTAL PLATFORM

In the two experiments, the Pioneer 3-DX robot, equipped with a UTM-30LX laser scanner, as shown in fig.14, was used

FIGURE 14. The Pioneer 3-DX robot.

to follow the planning result. The experiment's set of parameters were based on prior simulations, with the exception that the maximum observation range, was limited to 2m. To further verify the performance, we used the robot to follow all the path planning results. Here, an AMCL localization package was employed to localize the robot and a Virtual Vehicle path following algorithm [40] was employed to follow the given path. Note that the localization and the covariance were all generated by the AMCL. The localizability evaluations along the tracks, shown in fig.18-20 and fig.24-25, were calculated from the covariance.

B. SIMPLE INDOOR EXPERIMENT

To prove the performance of the proposed evaluation function, an experiment was first carried out in a simple indoor environment as shown in fig.15a. Note that generally the simpler the environment is, the worse the localizability might be.

Fig.15b shows the occupancy map drawn by the robot using a Simultaneous Localization and Mapping technology. In Fig.15b, we also show the three path planning results where the solid blue curve describes the new optimal path, the solid red curve describes the traditional one and the solid cyan curve describes the LM path, which was planned by the LM Method. Note that the LM Method highly relies on a manual parameter $T_{\text{bin}} \in [0, 1]$ to distinguish the traversable region from the environment, according to the localizability. Fig.15 shows the localizability map used in LM Method after applying a T_{bin} equal to 0.1. Here, the white region, accepted as a traversable region in path planning, indicates the high localizability region where the localizability is better than T_{bin}. On the other hand, the black region, accepted as an impassable region in path planning, indicates the low localizability region where the localizability is worse than T_{bin}. By balancing the risk of too small traversable region and the risk of path planning failure we choose the T_{bin} equal to 0.1. Then we get the path planning result as the cyan curves in both fig.15(b) and fig.16 show.

Fig.17a and fig.17b show the 3 optimal paths in the evaluation maps of $E(\|\delta_{\text{m\_}D}\|)$ and $E_\theta(\delta_{\text{m\_}\theta})$ respectively. It can

(a)

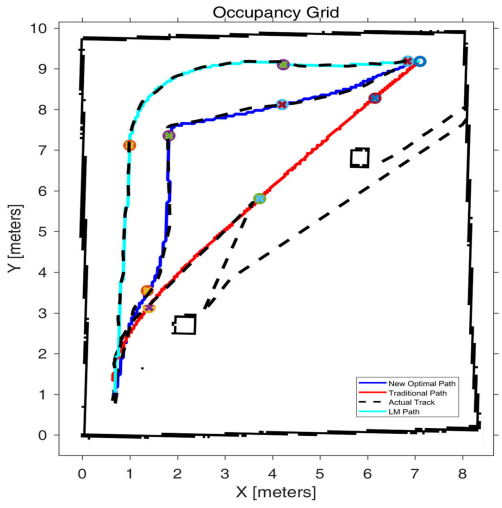

(b)

FIGURE 15. (a) The experiment environment (b) The occupancy grid map, paths and tracks.

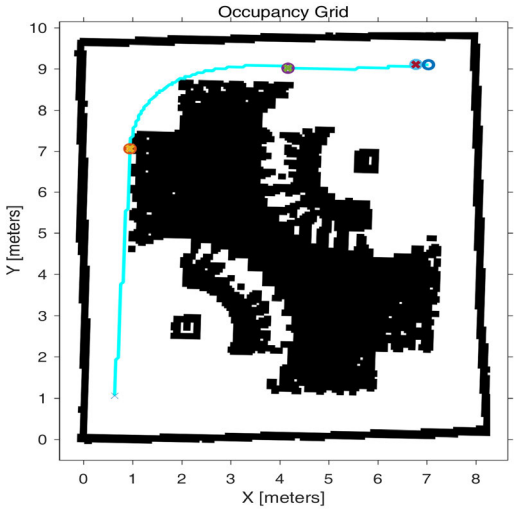

FIGURE 16. The localizability map used in LM method and the LM path.

easily be found that with our new evaluation function, the new optimal path has made a detour around the dense and black area in both the $E_\theta(\delta_{\text{m\_}\theta})$ map and the $E_\theta(\delta_{\text{m\_}\theta})$ map. However, the new optimal path has traveled through some black

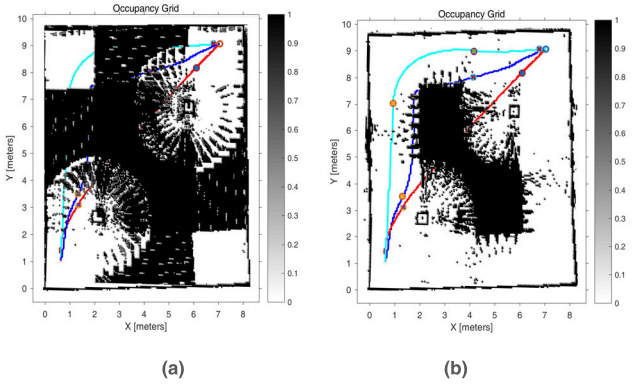

FIGURE 17. (a) The optimal paths in the map of $E(\|\delta_{m\_D}\|)$. (b) The optimal paths in the map of $E_\theta(\delta_{m_\theta})$.

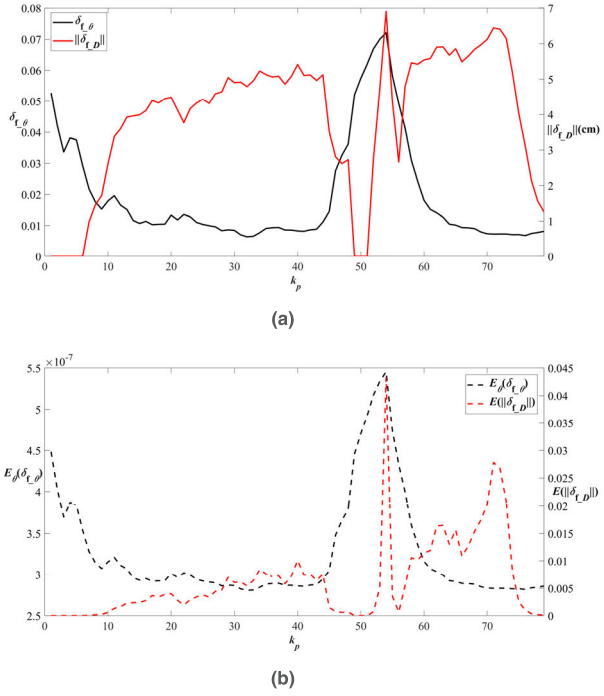

FIGURE 18. (a) δ_{f_θ} and $\|\delta_{f\_D}\|$ along the new optimal path. (b) $E_\theta(\delta_{f\_\theta})$ and $E(\|\delta_{f\_D}\|)$ along the new optimal path.

but sparse area of the maps to find a shorter path. By using the interspace inside the black area of the maps, the new optimal path can restrain the raising of the evaluation of the localizability by fusing the localization results from both dead-reckoning and map matching. In contrast, with the traditional evaluation function, the traditional optimal path is straighter and shorter in cost for traversing the low localizability areas in both the $E(\|\delta_{m\_D}\|)$ map and the $E_\theta(\delta_{m\_\theta})$ map for a long distance. As a result, the traditional optimal path most probably makes the robot gets lost in path following. LM path avoided the low localizability area in its localizability map shown in fig.4 as well. However, it can be found that the LM path is much longer than the new optimal path. This is because of two reasons. Firstly the localizability map used by LM method is a combination of our $E(\|\delta_{m\_D}\|)$ map

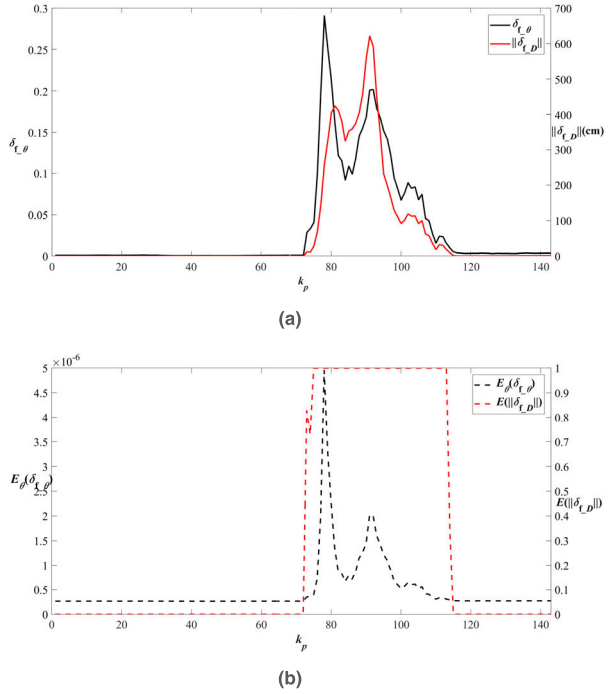

FIGURE 19. (a) δ_{f_θ} and $\|\delta_{f\_D}\|$ along the traditional optimal path. (b) $E_\theta(\delta_{f\_\theta})$ and $E(\|\delta_{f\_D}\|)$ along the traditional optimal path.

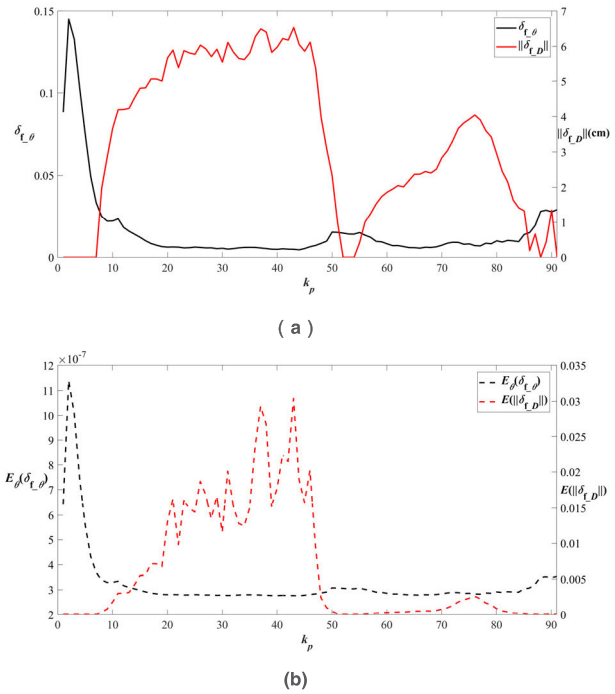

FIGURE 20. (a) δ_{f_θ} and $\|\delta_{f\_D}\|$ along the LM path. (b) $E_\theta(\delta_{f\_\theta})$ and $E(\|\delta_{f\_D}\|)$ along the LM path. (b) The optimal paths in the map of $E_\theta(\delta_{m\_\theta})$.

and $E_\theta(\delta_{m\_\theta})$ map, so that after the T_{bin} has been applied as a threshold, the traversable region may be differ than that in our method. Secondly, the LM method avoids traveling through any low localizability area because it has not taken into account the benefits from dead-reckoning.

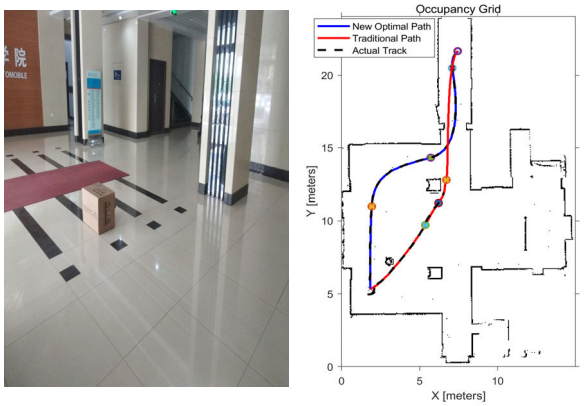

FIGURE 21. (a) The experiment environment (b) paths and tracks in the map.

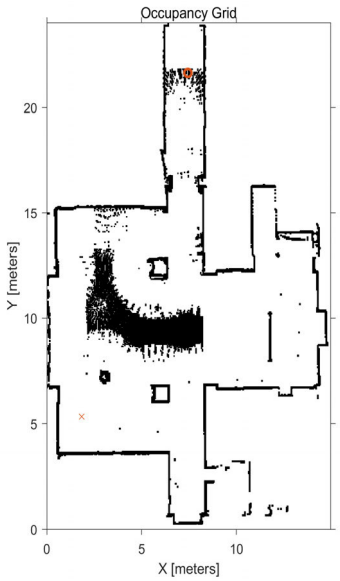

FIGURE 22. The localizability map for LM method.

Fig.15b also shows the actual track of the robot in experiment where the dotted curves close to the paths denotes the actual tracks of the robot in following the optimal paths. By following the traditional optimal path, the robot has lost itself after it has bypassed the lower obstacle in the picture. Getting lost happened at about 78s after the experiment began. By following the LM path, the robot successfully achieved the destination in 141s after it traveled about 15.2m. On the other hand, by following our new optimal path, the robot successfully achieved the destination in 130s after it traveled about 13.8m. Some divergences from the optimal paths have been observed in the three cases. These were mainly caused by two reasons. Firstly, the path following error comes from the Virtual Vehicle algorithm that makes an imperfect track. Secondly, the bad localizability region may bring bigger errors in localization and makes the actual track diverge from the given path.

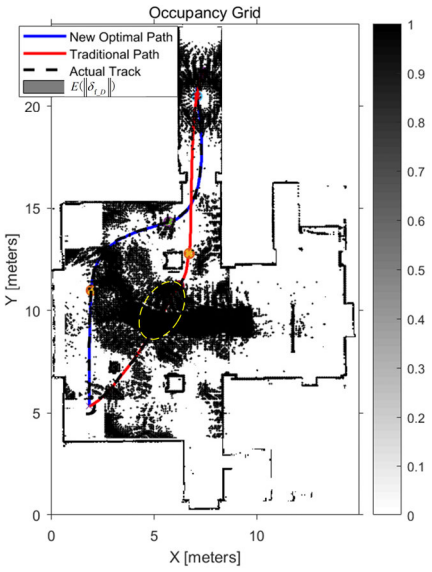

FIGURE 23. The paths and tracks in the map of $E(\|\delta_{m\_D}\|)$.

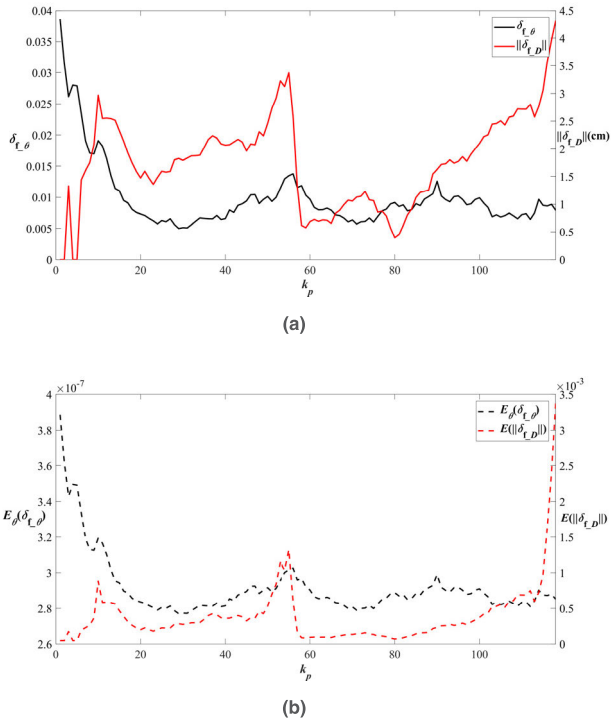

FIGURE 24. (a) δ_{f_θ} and $\|\delta_{f\_D}\|$ along the new optimal path. (b) $E_\theta(\delta_{f\_\theta})$ and $E(\|\delta_{f\_D}\|)$ along the new optimal path.

Fig.18 shows the four localizability evaluations along the track by following the new optimal path. It can be found that the four localizability evaluations all appeared to be very low, which made the robot follow the path to its destination safely. Fig.19 shows the four localizability evaluations along the track by following the traditional optimal path. In contrast, in the 75th location, a very big $\|\delta_{f\_D}\|$ was observed. As a result, the robot got lost and a big divergence from the given road was found. The robot could not escape from

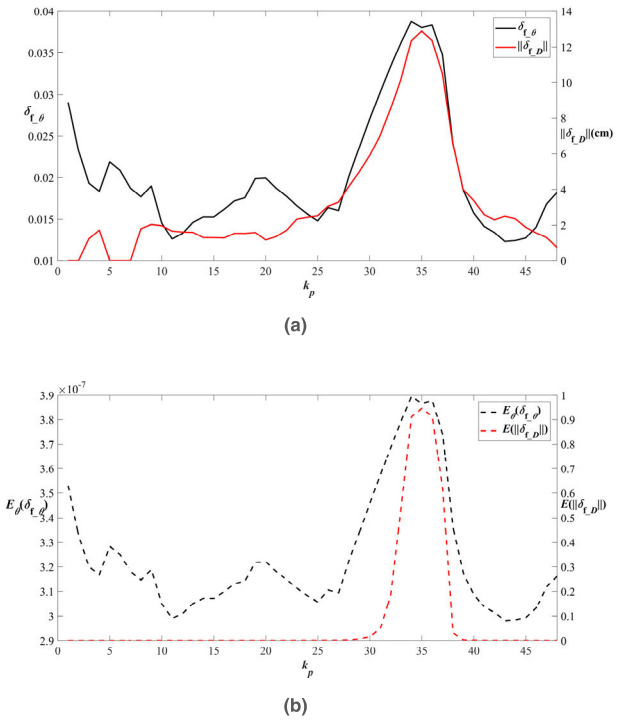

FIGURE 25. (a) $\delta_{\mathbf{f}\_\theta}$ and $\|\delta_{\mathbf{f}\_D}\|$ along the traditional optimal path. (b) $E_\theta(\delta_{\mathbf{f}\_\theta})$ and $E(\|\delta_{\mathbf{f}\_D}\|)$ along the traditional new path.

the random movements caused by the inaccurate localization result until the 115 th location. Fig.20 shows the localizability evaluations along the track of following the LM path. It can be found that LM path has also shown a good localizability along the path.

C. COMPLICATED INDOOR EXPERIMENT

To further investigate the performance of the proposed evaluation function, a more complicated experiment was conducted in a more complicated indoor environment. The environment's image and the occupancy map are given in fig.21. The distance between the two pillars in the figure is more than two meters which would cause big localization error in this experiment. As in the prior experiment, Fig.22 has shown a localizability map for the LM method after applying a T_{bin} equal to 0.00001. Unfortunately, the destination, shown as the circle in fig.22, is located inside a region with very bad localizability due to the simple surroundings. As a result, no matter how small the T_{bin} is, the LM method could not find an applicable path.

Fig.21 has also shown the actual track of the robot in experiment as the black dashed curve. Fig.23 has shown the paths and tracks in the map of $E(\|\delta_{\text{m}\_D}\|)$. We haven't shown the paths in the map of $E_\theta(\delta_{\text{m}\_\theta})$ because that map is mostly covered by the map of $E(\|\delta_{\text{m}\_D}\|)$. From fig.21 and 23, it can be found that the new optimal path, shown as the blue curve, is longer than the traditional path, shown as the red curve. However, fig.23 shows that the traditional path traveled through the black region for a long distance within the yellow dashed circle. As a result, by following the traditional path, the robot collided with the upper pillar in fig.21 due to localization error. The four key localizability evaluations, shown in fig.25, have also shown that the evaluation of the localizability had almost reached 1. In contrast, our new optimal path has made a detour to avoid traveling in the black region for too long a distance. The four key localizability evaluations, shown in fig.24, also showed that the new optimal path successfully brought a good localizability for the robot. As a result, the robot successfully achieved the destination after traveling about 20.44m. It can be found that when the destination is located inside a low localizability area without sufficient landmarks, the LM method could not find any applicable path while our method was capable to find an optimal one. The difference comes from two points. Firstly, the LM method avoids traveling through any low localizability area, while our method allows that. Secondly, the LM method employs Censi's theory to estimate the localizability which is only designed for map matching based localization. In contrast our method estimates the localizability not only from map matching but also from dead-reckoning. This means the low localizability area for LM method may not reflect the reality accurately. The tail part of the curves in fig.24 prove that the localizability may not be as bad as the black region in the map of $E(\|\delta_{\text{m}\_D}\|)$ shows.

VI. CONCLUSION

This paper mainly focused on the path planning for mobile robots while considering the impact of localizability. In our research, the uncertainty of localization has been studied by fusing the uncertainties that come from both map matching and dead-reckoning. Two models have been proposed to evaluate the negative impact of $\|\delta_D\|$ and δ_θ on path planning. Based on the two models a new evaluation function for path planning has been proposed. Both simulations and experiments have proved that compared with the existing research, our new evaluation function can offer better balancing among the localizability requirement, the traditional shorter path requirement and the safer path requirement.

The proposed approach employed the theory proposed by Censi [27] to estimate the localizability from map matching. However, this brings a time-consuming calculation of the upper bound of the localizability. So, a simpler and more direct way to estimate the localizability would be included in our future research. Moreover, this paper focuses on the localizability issue in a static environment only, which is based on the reality that for most localization methods, moving objects are generally excluded from the map. However, moving objects do bring impacts on localizability, so evaluate the localizability in a dynamic environment would be another challenge in our future research. Finally, many simplifications have been made in the analysis of the uncertainty in localization and its impact evaluation. So, a more accurate research about that would also be in our future interest.

REFERENCES

[1] P. K. Das, H. S. Behera, S. Das, H. K. Tripathy, B. K. Panigrahi, and S. K. Pradhan, "A hybrid improved PSO-DV algorithm for multi-robot path planning in a clutter environment," *Neurocomputing*, vol. 207, no. 1, pp. 735–753, 2016.
[2] M. Norouzi, J. V. Miro, and G. Dissanayake, "Planning stable and efficient paths for reconfigurable robots on uneven terrain," *J. Intell. Robot. Syst.*, vol. 87, no. 2, pp. 291–312, Aug. 2017.
[3] Y. Gao, S.-D. Sun, D. W. Hu, and L. J. Wang, "An online path planning approach of mobile robot based on particle filter," *Ind. Robot*, vol. 40, no. 4, pp. 305–319, 2013.
[4] J. L. Sanchez-Lopez, M. Wang, M. A. Olivares-Mendez, M. Molina, and H. Voos, "A real-time 3D path planning solution for collision-free navigation of multirotor aerial robots in dynamic environments," *J. Intell. Robot. Syst.*, vol. 93, nos. 1–2, pp. 33–53, 2019.
[5] A. K. Guruji, H. Agarwal, and D. K. Parsediya, "Time-efficient A* algorithm for robot path planning," *Procedia Technol.*, vol. 23, no. 1, pp. 144–149, 2016.
[6] J. Liu, J. Yang, H. Liu, X. Tian, and M. Gao, "An improved ant colony algorithm for robot path planning," *Soft Comput.*, vol. 21, no. 19, pp. 5829–5839, Oct. 2017.
[7] J. Lee and D.-W. Kim, "An effective initialization method for genetic algorithm-based robot path planning using a directed acyclic graph," *Inf. Sci.*, vol. 332, no. 1, pp. 1–18, 2016.
[8] W. Huang, C. Yan, J. Wang, and W. Wang, "A time-delay neural network for solving time-dependent shortest path problem," *Neural Netw.*, vol. 90, no. 1, pp. 21–28, 2017.
[9] J.-H. Zhang, Y. Zhang, and Y. Zhou, "Path planning of mobile robot based on hybrid multi-objective bare bones particle swarm optimization with differential evolution," *IEEE Access*, vol. 6, pp. 44542–44555, 2018.
[10] S. Hosseininejad and C. Dadkhah, "Mobile robot path planning in dynamic environment based on cuckoo optimization algorithm," *Int. J. Adv. Robot. Syst.*, vol. 16, no. 2, p. 1729881419839575, 2019.
[11] A. V. Savkin and H. Huang, "Optimal aircraft planar navigation in static threat environments," *IEEE Trans. Aerosp. Electron. Syst.*, vol. 53, no. 5, pp. 2413–2426, Apr. 2017.
[12] T. Urakubo, "Stability analysis and control of nonholonomic systems with potential fields," *J. Intell. Robot. Syst.*, vol. 89, no. 1, pp. 121–137, Jan. 2018.
[13] A. Babinec, F. Duchon, M. Dekan, Z. Mikulová, and L. Jurišica, "Vector field histogram* with look-ahead tree extension dependent on time variable environment," *Trans. Inst. Meas. Control*, vol. 40, no. 4, pp. 1250–1264, 2016.
[14] U. Orozco-Rosas, O. H. M. Ross, and R. Sepúlveda, "Mobile robot path planning using membrane evolutionary artificial potential field," *Appl. Soft Comput.*, vol. 77, pp. 236–251, Apr. 2019.
[15] F. Bayat, S. Najafi-Nia, and M. Aliyari, "Mobile robots path planning: Electrostatic potential field approach," *Expert Syst. Appl.*, vol. 100, pp. 68–78, Jun. 2018.
[16] S.-Y. Kim and Y. Yang, "A self-navigating robot using fuzzy Petri nets," *Robot. Auton. Syst.*, vol. 101, pp. 153–165, Mar. 2018.
[17] A. Gunathillake, H. Huang, and A. V. Savkin, "Sensor network based navigation of a mobile robot for extremum seeking using a topology map," *IEEE Trans. Ind. Informat.*, vol. 15, no. 7, pp. 3962–3972, Jul. 2019.
[18] J. Li, G. Deng, C. Luo, Q. Lin, Q. Yan, and Z. Ming, "A hybrid path planning method in unmanned air/ground vehicle (UAV/UGV) cooperative systems," *IEEE Trans. Veh. Technol.*, vol. 65, no. 12, pp. 9585–9596, Dec. 2016.
[19] M. Hank and M. Haddad, "A hybrid approach for autonomous navigation of mobile robots in partially-known environments," *Robot. Auto. Syst.*, vol. 86, pp. 113–127, Dec. 2016.
[20] T. T. Mac, C. Copot, D. T. Tran, and R. De Keyser, "Heuristic approaches in robot path planning: A survey," *Robot. Auto. Syst.*, vol. 86, pp. 13–28, Dec. 2016.
[21] S. G. Tzafestas, "Mobile robot control and navigation: A global overview," *J. Intell. Robot. Syst.*, vol. 91, no. 1, pp. 35–58, 2018.
[22] N. Roy, W. Burgard, D. Fox, and S. Thrun, "Coastal navigation-mobile robot navigation with uncertainty in dynamic environments," in *Proc. IEEE Int. Conf. Robot. Autom.*, vol. 1, May 1999, pp. 35–40.
[23] A. Alomari, F. Comeau, W. Phillips, and N. Aslam, "New path planning model for mobile anchor-assisted localization in wireless sensor networks," *Wireless Netw.*, vol. 24, no. 7, pp. 2589–2607, 2018.
[24] H. Wu, A. Ding, W. Liu, L. Li, and Z. Yang, "Triangle extension: Efficient localizability detection in wireless sensor networks," *IEEE Trans. Wireless Commun.*, vol. 16, no. 11, pp. 7419–7431, Sep. 2017.
[25] Z. Yang, C. Wu, Z. Zhou, X. Zhang, X. Wang, and Y. Liu, "Mobility increases localizability: A survey on wireless indoor localization using inertial sensors," *ACM Comput. Surv.*, vol. 47, no. 3, pp. 1–34, 2015.
[26] K. Qian, X. Ma, F. Fang, X. Dai, and B. Zhou, "Mobile robot self-localization in unstructured environments based on observation localizability estimation with low-cost laser range-finder and RGB-D sensors," *Int. J. Adv. Robot. Syst.*, vol. 13, no. 5, p. 1729881416670902, 2016.
[27] A. Censi, "On achievable accuracy for range-finder localization," in *Proc. IEEE Int. Conf. Robot. Autom.*, Apr. 2007, pp. 4170–4175.
[28] Y. Wang, W. Chen, J. Wang, and H. Wang, "Active global localization based on localizability for mobile robots," *Robotica*, vol. 33, no. 8, pp. 1609–1627, 2015.
[29] A. Ruiz-Mayor, J.-C. Crespo, and G. Trivino, "Perceptual ambiguity maps for robot localizability with range perception," *Expert Syst. Appl.*, vol. 85, no. 1, pp. 33–45, Nov. 2017.
[30] W. Zhen, S. Zeng, and S. Soberer, "Robust localization and localizability estimation with a rotating laser scanner," presented at the IEEE Int. Conf. Robot. Automat. (ICRA), Singapore, 2017.
[31] J. P. Gonzalez and A. T. Stentz, "Planning with uncertainty in position using high-resolution maps," in *Proc. IEEE Int. Conf. Robot. Autom.*, Apr. 2007, pp. 1015–1022.
[32] C. Hu, W. Chen, J. Wang, and H. Wang, "Optimal path planning for mobile manipulator based on manipulability and localizability," in *Proc. IEEE Int. Conf. Real-Time Comput. Robot. (RCAR)*, Jun. 2016, pp. 638–643.
[33] S. Robert, B. Peter, and C. Stachniss, "Efficient path planning in belief space for safe navigation," in *Proc. IEEE/RSJ Int. Conf. Intell. Robots Syst. (IROS)*, Vancouver, BC, Canada, Sep. 2017, pp. 2857–2863.
[34] B. Irani, J. Wang, and W. Chen, "A localizability constraint-based path planning method for autonomous vehicles," *IEEE Trans. Intell. Transp. Syst.*, vol. 20, no. 7, pp. 2593–2604, Jul. 2019.
[35] G. Q. Li, Y. H. Geng, and W. Z. Zhang, "Autonomous planetary rover navigation via active SLAM," *Aircr. Eng. Aerosp. Technol.*, vol. 91, no. 1, pp. 60–68, 2019.
[36] T. Sebastian, B. Wolfram, and F. Dieter, *Probabilistic Robotics*. Cambridge, MA, USA: MIT Press, 2005.
[37] Z. Liu, W. Chen, Y. Wang, and J. Wang, "Localizability estimation for mobile robots based on probabilistic grid map and its applications to localization," in *Proc. IEEE Int. Conf. Multisensor Fusion Integr. Intell. Syst. (MFI)*, Sep. 2012, pp. 46–51.
[38] Y. Gao, H. Xu, M. Hu, J. Liu, and J. Liu, "Path planning under localization uncertainty," *J. Eur. Syst. Autom.*, vol. 50, nos. 4–6, pp. 435–448, 2017.
[39] M. Egerstedt, X. Hu, and A. Stotsky, "Control of mobile platforms using a virtual vehicle approach," *IEEE Trans. Autom. Control*, vol. 46, no. 11, pp. 1777–1782, Nov. 2001.

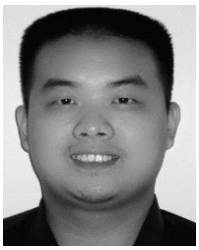

YANG GAO received the Ph.D. degree in mechatronics engineering from Northwestern Polytechnic University, Xi'an, China, in 2011. He is currently an Associate Professor with the Automobile College, Chang'an University, and a Visiting Scholar with the University of Illinois at Chicago. His research interests include robotics, navigation of mobile robot, simultaneous localization and mapping (SLAM), and control system design of DC motors.

JIANG LIU received the bachelor's degree in vehicle engineering from the Tianjin University of Science and Technology, Tianjin, China, in 2017. He is currently pursuing the master's degree with the Automobile College, Chang'an University. His research interests include intelligent vehicle control, and mobile robot path planning and navigation.

MENG QI HU received the Ph.D. degree in industrial engineering from Arizona State University, USA, in 2012. He is currently an Assistant Professor with the Department of Mechanical and Industrial Engineering, The University of Illinois at Chicago. His research interests include complex system design and optimization, distributed decision support and analysis, swarm intelligence and evolutionary computation, meta-learning, and meta-modeling.

HAO XU received the bachelor's degree in vehicle engineering from the Shandong University of Science and Technology, Qingdao, China, in 2016. He is currently pursuing the master's degree with the Automobile College, Chang'an University. He is studying intelligent vehicle control, multisensor data fusion, robot positioning, and path planning. He is currently focusing on multisensor data fusion of mobile robots.

KUN PENG LI received the bachelor's degree in vehicle engineering from the Tianjin University of Science and Technology, Tianjin, China, in 2018. He is currently pursuing the master's degree with the Automobile College, Chang'an University. His study is mainly focused on SLAM technology, and mobile robot path planning and navigation.

HUI HU received the Ph.D. degree in system engineering from Beijing Jiaotong University, Beijing, China, in 2008. She is currently an Associate Professor with the Automobile College, Chang'an University. She mainly focuses on robot system optimization and artificial intelligence.